One-Step Fabrication of GeSn Branched Nanowires

Jessica Doherty[1,2], Subhajit Biswas[1,2], David McNulty[1], Clive Downing[3], Sreyan Raha[4], Colm O'Regan[5], Achintya Singha[4], Colm O'Dwyer[1] and Justin D. Holmes[1,2*]*

[1]School of Chemistry, ERI and the Tyndall National Institute, University College Cork, Cork, Ireland, T12 YN60. [2]AMBER@CRANN, Trinity College Dublin, Dublin 2, Ireland. [3]Advanced Microscopy Lab, Trinity Enterprise Centre, Pearse Street, Dublin 2, Ireland. [4]Department of Physics, Bose Institute, Kolkata, India. [5]NABLA Lab, Biological and Environmental Sciences and Engineering (BESE) Division, King Abdullah University of Science and Technology (KAUST), Thuwal 23955-6900, Kingdom of Saudi Arabia.

RECEIVED DATE (to be automatically inserted after your manuscript is accepted if required according to the journal that you are submitting your paper to)

Correspondence and requests for materials should be addressed to JDH (email: j.holmes@ucc.ie) or to SB (email: s.biswas@ucc.ie).

Abstract

We report for the first time the self-catalysed, single step growth of branched GeSn nanowires by a catalytic vapour-liquid-solid (VLS) mechanism. These typical GeSn nanostructures consist of <111> oriented Sn rich (~8 at. %) GeSn "branches" grown epitaxially on GeSn "trunks", with a Sn content of ~ 4 at. %. The trunks are seeded from $Au_{0.80}Ag_{0.20}$ nanoparticles followed by the catalytic growth of secondary branches (diameter ~ 50 nm) from the excess of Sn on the sidewalls of the trunks, as determined by high resolution electron microscopy and energy dispersive X-ray (EDX) analysis. The nanowires, with <111> directed GeSn branches oriented at ~ 70 ° to the trunks, have no apparent defects or change in crystal structure at the trunk-branch interface; structural quality is retained at the interface with epitaxial crystallographic relation. Electrochemical performance of these highly ordered GeSn nanostructures were explored as a potential anode material for Li-ion batteries, due to their high surface to volume ratio and increased charge carrier pathways. The unique structure of branched nanowires led to high specific capacities comparable to, or greater than, conventional Ge nanowire anode materials and $Ge_{1-x}Sn_x$ nanocrystals.

Keywords: Nanowires, germanium-tin, branched nanostructure, Li-ion battery

Introduction

The high surface-to-volume ratios of branched nanowires makes them ideal candidates for a number of applications, such as photovoltaics,[1–3] water splitting[4,5] and as electrode materials in batteries.[6–8] The radial growth of nanowire "branches" from the primary nanowire "trunk" represents a route to form higher faceted structures, with capabilities beyond the remit of one dimensional nanowires.[9,10] Branched nanostructures can be engineered from the same material (homostructures) or from different materials forming the trunk and branch segments (heterostructures).[1,8,11] These nanostructures can be highly ordered and the branches can be preferentially controlled[12,13] and could behave as a three-dimensional nanowire network.[14] Conventionally, branched nanowires, both heterostructured and homostructured, have been fabricated by two-step approaches. Typically, the trunks are grown first, followed by the generation of branches on the surface of the trunks using a secondary catalyst.[8,10,15] There have also been reports of branched nanowires grown in a single step through a "self-catalytic" process, either by segregation of a growth material towards the nanowire sidewall,[3,16] or by deposition of the initial catalyst onto the sidewalls.[2] A single step[1,3,16] growth protocol for any homo- or heterostructure formation has the advantage of simplicity, cost-effectiveness, phase purity and improved crystal quality over the heterostructure grown in a multi-step process.

In recent years, there has been a surge in interest surrounding GeSn alloy nanosystems.[17–20] Much of this interest has been due to reports, both theoretical and experimental, that a direct bandgap can be achieved in Ge by alloying the semiconductor with Sn,[21,22] lowering the separation between the indirect (L) and direct (Γ) valleys (140 meV in bulk Ge) in the conduction band of Ge.[23] While there have been numerous reports on the fabrication and characterisation of GeSn thin films,[24–28] researchers are still in the early stages of exploring

GeSn nanoystems. The generation of $Ge_{1-x}Sn_x$ ($x \approx 0.06$-0.20) nanowires have previously been reported *via* both top-down fabrication[29,30] and bottom-up growth,[31–33] and GeSn nanocrystals have been reported with up to 40 at. % Sn incorporation.[34–37] Considering group IV branched nanostructures, there have been demonstrations of branched nanowires comprising of Si[38] and Si/Ge,[8] however, to the best of our knowledge, there are no reports of GeSn alloy branched nanowires. Particularly, branched GeSn nanostructures could have potential in many different optoelectronic and nanoelectronic applications, due to their unique material characteristics and novel morphology. GeSn branched nanostructures, with direct and narrow band gaps and high surface areas, have potential application in efficient light absorption and as high mobility materials in 3D nanowire networks. GeSn alloy branched nanostructures could potentially act as both type-I and type-II semiconductor heterojunctions,[9] where the bandgap of the branch and trunk segments could be controlled *via* the variation in Sn incorporation.

Branched GeSn alloy nanowires are also good candidates for energy storage applications due to the integration of different functional materials, greatly enhanced numbers of junctions, large surface areas and high carrier mobility.[7,39] For energy storage, Sn-catalysed Ge nanowires have been previously reported to demonstrate high capacities when used as an anode material for Li ion batteries,[40] and GeSn nanocrystals with 5 at. % Sn have shown improvement in capacitance and retention over Ge nanocrystals.[34] This, combined with the high surface area, increased charge carrier pathways and strong mechanical strength,[39,41] suggest that GeSn branched nanowires may exhibit high capacities when used as an anode material in Li ion batteries.[6,8,15]

This article reports for the first time the vapour-liquid-solid (VLS) growth of branched GeSn nanowires using $Au_{0.80}Ag_{0.20}$ alloy nanoparticles as catalytic seeds. We exploited the

conventional VLS growth paradigm to access the growth of branched GeSn heterostructures with crystalographically perfect interfaces. The 3D nanostructures exhibit heterogeneity in terms of Sn content variation between the trunks and the branches. The quality of the interface in the branched structures in terms of Sn distribution, crystal defects, epitaxy, *etc.* was analysed using high resolution scanning transmission electron microscopy (HRSTEM) and energy dispersive x-ray (EDX). A growth mechanism for the nanostructures is proposed taking account of growth constraints such as catalysts, precursors *etc*. The potential application of the branched GeSn nanowires as anode materials for Li ion batteries is also discussed.

Results and Discussion

For the growth of GeSn alloy branched nanostructures, a conventional, single step VLS growth mechanism was employed where a particular combination of catalyst, Sn precursor type and concentration resulted in the nucleation and epitaxial growth of small GeSn nanowires from the sidewalls of large GeSn nanowire trunks (see Supporting Information for detailed experimental methods). Using previously reported[42] Ge and Sn precursor sources (diphenyl germane (DPG) and tetraethyl tin (TET) as Ge and Sn source respectively) and $Au_{0.80}Ag_{0.20}$ nanoparticles as the catalyst, an extensive amount of branched GeSn alloy nanowires were produced, as shown in the scanning electron microscopy (SEM) image in Figure 1(a). Calculating an accurate yield of the branched structure was difficult, due to the depth of the deposited film and difference in the dimension of the branched and unbranched nanowires. The branches in the GeSn nanowires produced were highly uniform, in terms of diameter (57 ± 14 nm), and highly ordered along the length of the nanowire trunks (Figure 1(b)). The mean diameter of trunks was found to be 248 ± 85 nm. SEM analysis of the GeSn branches suggested that in some instances there was no apparent growth seed visible at the tip of the branches

(Figure 1(b)), whereas in other nanostructures, metal seeds were visible at the tips (Figure 1(c) , red arrows to indicate presence of seeds). A TEM image showing nanowire branches with metal seeds is shown in inset of the figure for further clarification. Also visible in Figure 1(c) are small spherical seeds on a large nanowire trunk, and the growth of short branch nanowires on another trunk. Spherical metal tips are also clearly visible in many of the nanowire trunks shown in Figure 1(d). Figure 1(d) also depicts the increasing length of the branches along the length of the primary trunk, *i.e.* the branches closest to a nanowire seed are shorter in length than those further away from a seed (yellow lines are used as a guide for the eyes). The lengths of the nanowire branches along a single trunk ranged from a few tens of nanometres to almost a micron. Although there is no conclusive trend on the density of the branching on the size of the branched nanostructure, a comparatively higher density of branching with thicker trunk segment seems to be the common feature of these branched nanostructures (Supporting Info, Figure S1). Accurate estimation of the density of branching of the nanostructures is limited with the 2-D representation of the SEM image.

EDX point analysis of multiple branched nanowires revealed the mean Sn content in the trunks (4.4 ± 0.7 at. % Sn) to be significantly less than in the branches of the same nanostructure (8.0 ± 1.2 at. % Sn) (Supporting Info, Figure S2). An elemental map and the associated spectra for a nanowire trunk body at the seed/nanowire interface can be seen in Figure 2(a) (Au denoted by red, Sn by green and Ge by purple). The Au component in the metallic tip can be identified in the nanowire seed by presence of a bright red spot at the tip of the seed. The sharp interface typical of $Ge_{1-x}Sn_x$ nanowires grown using our method is observable, with no obvious signs of Sn segregation at the growth interface.[42,43] The Sn-rich nature of the catalytic seed post-growth has previously been reported for GeSn nanowire growth.[42,43] The accompanying spectra from the trunk nanowire seed confirms the presence of Au and Ag in the catalyst seed with no

evidence of Au or Ag diffusion into the branched nanostructure (Figure S2 in Supporting Information) Uniform distribution of Sn and Sn spherical tip is also apparent from the EDX elemental maps (Ge denoted by blue and Sn denoted by red) and corresponding HAADF STEM image of a branch segment of the nanostructure ((Figure 2(b)). In order to determine the contribution of the different catalyst seeds ($Au_{0.80}Ag_{0.20}$ and Sn) in the growth of the trunk and branch elements of these nanowires, EDX analysis of the seeds were carried out on both trunk and branch components. While the spectrum from a trunk nanowire seed clearly demonstrates the presence of the Au and Ag in the catalyst tip (Supporting Info, Figure S3 and), the EDX spectrum from a branch nanowire seed contains no apparent Au or Ag signal, but is comprised solely of Ge and Sn.

Incorporation of Sn in the trunk and the branch segments of the GeSn nanostructures is further confirmed by Raman spectroscopy on individual branched nanostructures. Measurements were undertaken on three different branched nanostructures ((Figure 2(c)) and Figure S4 in Supporting Information) where the nanostructures were transferred to a carbon coated Cu grid. A single Ge-Ge Raman peak from GeSn nanowire alloys has been previously observed to progressively shift to a lower energy with increasing Sn concentration.[43] However, unlike conventional GeSn nanowires, Raman spectra from the GeSn branched nanostructures (Figure 2(c)) shows two distinct peaks (blue line denotes Lorentzian fitting) at higher (centred at 298.7 cm^{-1} by averaging position of three different spectra) and lower (centred at 289.2 cm^{-1} by averaging position of three different spectra) wavenumbers. These two peaks can be related to the variation in Sn content between the trunk and the branch components of the nanostructure. The relatively more intense Ge-Ge LO peak at lower frequency shows a red shift of approximately 4.3 cm^{-1} , assuming a standard bulk Ge peak centred at 303 cm^{-1} peak.[42] This relatively intense Ge-Ge LO vibration can be assigned to the trunk segment of the

nanostructure, with a large volume and with low Sn content (4.4 at. % Sn), as the peak position matches well with previously reported GeSn alloys with similar Sn incorporation.[44,45] The second Ge-Ge LO peak at much lower frequency, approximately 13.8 cm^{-1} red shifted from the bulk Ge-Ge vibration, can be attributed to the GeSn branches with a high Sn composition (8.0 at. % Sn). The red shift of Ge-Ge LO mode was more prominent than that observed previously in conventional GeSn nanowires with a similar Sn content.[42,43] However, apart from the Sn alloying effect, the shift of the Ge-Ge frequency in the Raman spectra can also occur from the strain effects and alloy disorder[42,43], which may have had an effect on the observed Raman shift. A Raman mode arising from a Ge-Sn bond, usually appearing around 260 cm^{-1}, was not observed in the spectrum from the GeSn branched nanostrutures.

The structural quality of the GeSn nanowires was determined by STEM in high angle annular dark field (HAADF) mode (Figure 3). Representative HAADF STEM images of a branch-trunk interface and a nanowire branch containing a metal seed at the tip are shown in Figures 3(a) and (b) respectively. The interface between the nanowire trunk and branch is also depicted in the high resolution STEM image in Figure 3(c). The branches clearly stem from the main nanowire trunk, with no twin boundaries or other crystal defects, such as stacking faults, apparent at the interface. For the particular branch segment shown in Figure 3(a) the angle between the trunk and the branch was 71.6 °, in agreement with the minimum angle between two <111> directions in a cubic crystal arrangement and also previously observed for <111> nanowires grown from a (111) surface (70.53°),[46] as well as between nanofacets in twin boundaries in <111> Ge nanowires.[47] A similar crystallographic orientation between branch and trunk nanowire components is apparent in Figure 3(c), where an extension of {111} stacking in the trunk segment is observed in the branch component, where the branches grow along {111} equivalent directions. The apparent continuity in the lattice from the trunk to the

branch segments further confirms epitaxial orientation of the branch segments from the trunks. The two-dimensional projection of the nanostructure during STEM imaging and the presence of a thin oxide layer, make the accurate determination of the angle between branch and trunk segments difficult. Fast Fourier Transform (FFT) analysis of a nanowire (Figure 3(c) inset) revealed the interplanar spacing (*d*) close to the interface to be 0.32 nm, which is in agreement with the *d* value for bulk diamond Ge crystal of 0.326 nm (JCPDS 04–0545). The interplanar spacing for both a nanowire trunk (0.32 nm) and a nanowire branch (0.35 nm) revealed discrepancies resulting from differences (approx. 4 at. %) in the Sn contents in the different segments. The branch nanowires predominantly displayed a <111> growth direction, the most common growth orientation for Ge nanowires with the mean diameter above 50 nm.[43,48] Generally the crystal structure of the $Ge_{1-x}Sn_x$ alloy branched nanowires, with various Sn incorporations, exhibited a 3C lattice arrangement without any stacking faults and twin boundaries. This non-appearance of any crystal imperfections could be due to the minimal lattice mismatch between the branch and trunk segments and the accommodation of strain through sidewall facets due to the high surface-to-volume ratio of the thin GeSn branch components.

The small hemispherical seed of the branched nanowire, highlighted in the green box of Figure 3(b), is shown at higher resolution in Figure 3(d). There is a clearly observed, well-defined interface between the metal seed and the nanowire body. Also apparent is an amorphous bulb surrounding the small seed (indicated by the orange arrow, Figure 3(d)). This bulb has been previously observed in $Ge_{1-x}Sn_x$ nanowire growth and is comprised of a GeSn oxide with high Sn content.[42] The relative size of this bulb compared to the crystalline seed which it encompasses makes precise EDX analysis of the branching seed difficult. However, measuring the lattice spacing of the hemispherical tip segment gives an interplanar spacing (*d*) of 0.29

nm, which corresponds well with the {200} plane of metallic Sn (JCPDS cards #04–0673). This hemispherical seed at the tip of the branch elements was not apparent in all branched nanowires studied in this work (Figure 1(b), and Figure S5(a) in Supporting Info,). In some cases, there was evidence of a small seed of reduced dimension, visible only due to the difference in the contrast between the branch nanowire body and the metallic seed (Supporting Info, Figure S5(b)). Usually the branched nanowires display metallic seeds at the tip of the shorter branches with longer branches along the length of the primary nanowire trunk having little to no observable metallic seeds (Supporting Info, Figure S6). Metallic Sn seeds which are categorised as low-surface energy, type-B metallic seeds in VLS growth, can demonstrate prominent wetting at the liquid-solid interface.[3,16] This wetting leads to gradual reduction in the seed volume and disappearance from the nanowire tip during VLS growth. Similar observations on the appearance of metal seeds have previously been observed for single step branched nanowires,[3] grown from Pb seeds.

Precise control over the growth of branched nanowires, *e.g.* length, diameter, epitaxy, density, Sn content, *etc*., is useful for future device (*e.g.* in photovoltaics) implementation. In order to engineer the extent of branching in the nanowires, and to determine the growth mechanism of these Sn-alloyed Ge nanostructures, time-dependent growth experiments were undertaken. Experiments were carried out under typical growth constraints with varying reaction times (15, 30, 45, 60, 80, 100 and 120 min). Information on the morphologies of the nanostructures through TEM imaging, EDX elemental mapping and schematics of typical nanowire growth scenario at 30, 80 and 120 min are provided in Figure 4. A build-up of Sn nanoparticles on the sidewalls of the nanowire trunk is apparent after 30 min of growth time, as determined from TEM analysis (Figure 4(a) and (b)) and EDX elemental mapping (Figure 4(c)). In Figure 4(a), nanoparticle-like clusters can be seen segregating/migrating from the nanowire seed toward the

seed/nanowire interface and the nanowire sidewall (indicated by blue circles). This Sn diffusion from the seed triggers the secondary growth of branch nanowires. In Figure 4(b), a dark contrasted nanoparticle can be clearly seen (indicated by blue circle) on the sidewall of a primary nanowire trunk. The formation of large Sn rich cluster on the sidewall of the trunk nanowire (Figure 4(c) – with Sn denoted by red and Ge by green) is also apparent. Due to the limited growth time, the nanowire yield across the substrate after a 30 min reaction time was quite low (Supporting Info, Figure S7(a)). The growth of branched nanowire segments was initiated after a reaction time of approximately 80 min (Figure 4(d) and Supporting Info, Figure S7(b)). TEM analysis confirmed the growth of short (< 100 nm) branched nanowires after 80 min growth, with the presence of a growth seeds at the tip of the branches. Some nanowire trunks also showed the formation of a layer at the surface of the nanowire trunks after 80 min growth (Figure S8 in Supporting Info). The lattice spacing of the crystalline edge of this shell (2.88 Å) is consistent with metallic Sn. This Sn rich surface of the nanowire trunk after 80 min growth indicates Sn wetting on the sidewall of the main trunk segment, either from the large metallic seed or through direct deposition of Sn from the precursor vapour phase. These Sn nanoparticles further act as the seeding location for the secondary growth of GeSn nanowire branches on primary trunk segments. Representative SEM images of GeSn nanostructures after 30 and 80 min growth times are provided in Supporting Info, Figure S7. The schematic shown in Figure 4(e) represents a branched nanowire at 30, 80 and 120 min growth times (representative SEM image for 120 min growth is in Figure 1(a)). The branched nanowire lengths in the schematic have been emphasised for illustrative purposes. The schematic is presented as a visible representation for better understanding of branched nanowire growth only and is not a scientifically accurate drawing in terms of nanowire facets, shape of the metallic particles and interface geometry.

As no intentional catalyst was added to break the isotropic GeSn crystal growth to fabricate branched nanostructures, an understanding of the mechanism responsible for this growth is imperative for the controlled fabrication of branched nanowires. There are three possible sources for the origin of the Sn rich outer layer (Figure 4 and Figure S8 in Supporting Info) which acts as the seed for secondary growth of nanowire branches on the sidewalls of the GeSn trunks. The excess Sn on the nanowire sidewalls could originate from: (i) Sn segregation from the bulk of a nanowire trunk, (ii) Sn deposition and droplet formation on the sidewalls of nanowire trunks from the external continuous flux of Sn during growth and (iii) the wetting and migration of the Sn from the metallic tip of the nanowire trunk to the nanowire sidewalls. Among these mechanisms, Sn segregation from the nanowire bulk is not justified as uniform Sn distribution is observed in the trunk nanowire body (Figure 2(c)), suggesting no migration of Sn from the nanowire bulk to the surface. Also stable $Ge_{1-x}Sn_x$ alloy nanowires with higher Sn concentration ($x = 0.09$) have been reported[42] using a similar growth technique without any apparent segregation of Sn to the nanowire sidewalls. As Sn segregation at the surface of a nanowire trunk from its bulk is unlikely at a Sn content of ≈ 4 at. %. Sn accumulation on the sidewalls of the GeSn nanowire trunks can occur *via* both the spontaneous deposition of Sn from Sn precursor and migration of smaller particles from the primary catalyst particle at the tip of the trunk. Although at the growth temperature employed (440 °C), the solubility of Sn in AuAg catalyst is limitless, but beyond a threshold volume of the catalyst, small Sn nanoparticle droplet can precipitate out from the liquid seed to wet the sidewalls of the nanowires (Figure 4 (a) and (b)). This is due to the formation of Sn-rich metastable catalyst particles (Figure 2(c)) with low surface energies at the growth temperature. In this study, the nanoparticle catalyst, Sn precursor and its concentration was found to have a real impact on the yield of branched nanostructures compared to the non-branched nanowires (See method in Supporting Info). The $Au_{0.80}Ag_{0.20}$ nanoparticle catalyst was found to be a crucial parameter

in the formation of the branched nanostructures (Figure 1(a) and Figure S9 in Supporting Informaiton). Ag-rich, AuAg seeds at a growth temperature of 440 °C require a larger Sn solubility to form the liquid Au, Ag and Sn alloy eutectic (according to the phase diagrams of Au-Sn[49] and Ag-Sn[50]). With high Sn solubility, it may be argued that the threshold volume (volume beyond which Sn precipitates from the seed) of the eutectic catalyst in the trunk nanowire is reached more readily for a $Au_{0.80}Ag_{0.20}$ catalyst compared to pure Au, resulting in Sn nanoparticle droplet formation and the observation of a high yield of branched nanowires for $Au_{0.80}Ag_{0.20}$ catalysts.

In another scenario, Sn can be directly adsorbed from the vapour phase, both at the spherical catalyst and at the faceted nanowire surface (a cross-sectional image of GeSn branched nanowire trunk can be seen in Supporting Info, Figure S10). In VLS growth, adsorption of the growth species at the eutectic catalyst is typically influenced by the difference in the adatom concentration in the vapour and liquid phases. Thus, for a certain Sn precursor concentration in the vapour phase, the difference in the Sn adatom concentration between vapour and liquid phases is smaller for the $Au_{0.80}Ag_{0.20}$ catalyst (due to larger Sn solubility) resulting in slow adsorption at the vapour-liquid interface. This slow adsorption rate may result in an excess Sn adatoms in the growth environment, which triggers Sn accumulation directly on the sidewalls of the nanowire trunks, or at the eutectic droplets. Accumulated Sn at the surface of the eutectic droplet (apart from the precipitated Sn from the catalyst) can also migrate to the nanowire sidewalls. This Sn at the nanowire sidewalls can act as growth catalyst, resulting in the continuous growth of the nanowire branches during the simultaneous growth of the nanowire trunks (Figure 1(d)). Though both mechanism (ii) and (iii) could be liable for the formation of branched nanowires, it can be argued that accumulation/precipitation and migration of Sn droplets from the seed could be a more prominent mechanism. Observation of very regular

and oriented branching and very little observation of uncontrolled hyper branches in fully grown branched structure (Figure 1) disprove the participation of uncontrolled and direct Sn deposition on the nanowire sidewalls from the vapour phase. These branched nanowires continue to grow until the Sn catalyst is consumed, leaving some branched nanowires with little to no evidence of a seed (Figure 1(b), Supporting Info, Figure S5). A similar outcome has been observed for the growth of single step tin oxide nanowires[16] where small secondary seeds were also observed on the sidewalls of nanowire trunks with no addition of external catalyst.

A further increase in the Ag content in the in AuAg alloy seeds, *e.g.* $Au_{0.70}Ag_{0.30}$, resulted in very few branched nanostructures (Supporting Info, Figure S9). This may be due to the vastly altered growth kinetics with the increased Ag content of the catalytic seeds, ultimately leading to very little growth of $Ge_{1-x}Sn_x$ nanowires.[42] The proposed growth mechanism for branched nanostructures is also supported by the, seemingly counter-intuitive, observation that an increase in the concentration of TET used as the Sn precursor (from 3 mmol/cc to 5 mmol/cc) resulted in a dramatic decrease in the yield of branched nanostructures.[42] The increased partial pressure of Sn with an increasing amount of the growth precursor would result in an increased Sn adsorption at the vapour-liquid interface during VLS growth, allowing for more Sn incorporation at the triple phase interface and in the nanowire *via* solute trapping,[42] rather than accumulation of Sn on the surface of the nanowire or eutectic catalyst.

The integration of different functional materials, greatly enhanced junctions and high surface areas make branched nanostructures good candidates for energy storage devices.[6,8,15] Galvanostatic cycling at a rate of 0.2 C, over a voltage range of 1.50 to 0.01 V (vs Li/Li^+) was

performed in order to investigate the fundamental electrochemical performance of the branched GeSn nanowires, as shown in Figure 5. A selection of voltage profiles from the 1st to the 25th cycle are shown in Figure 5(a). The 1st charge curve consists of an initial sharp decrease from the open circuit voltage (OCV) of ~3.10 V down to ~ 0.33 V, which may be attributed to the formation of a solid-electrolyte interface (SEI) layer and the irreversible decomposition of the electrolyte on the surface of the electrode material,[51] followed by 3 long plateaus from ~0.33 to 0.25 V, 0.25 to 0.16 V and from 0.16 V to 0.01 V, corresponding to the progressive lithiation of the branched GeSn nanostructures.[52] A long plateau centred at ~ 0.5 V was observed in the first discharge curve, corresponding to the delithiation of the nanostructures.[53] The initial charge and discharge capacities were ~ 1298 and 1079 mAh/g, corresponding to an initial Coulombic efficiency (ICE) of 83 %. The exceptional capacity retention properties of the branched nanostructures are demonstrated in Figure 5(b). The charge capacities after the 2nd and 25th cycles were 1107 and 1040 mAh/g respectively, corresponding to an impressive capacity retention of 94 %.

Differential capacity plots (DCPs) were calculated for each charge and discharge curve in order to fully appreciate the electrochemical processes occurring during galvanostatic cycling. DCPs for the 1st charge and discharge are shown in Figure 5(c). The sharp peak in the DCP for the 1st charge at 0.31 V is due to the lithiation of crystalline Ge (c-Ge)[54,55] and is only observed during the first charge, indicating that the nanowires do not return to a fully delithiated crystalline Ge phase.[54] The other peaks at ~ 0.17 and 0.13 V are associated with the formation of Li-Ge alloys in the form of a-$Li_{15}Ge_4$ and c-$Li_{15}Ge_4$, respectively.[56] From the second charge onwards, reduction peaks were observed at ~ 0.52, 0.39 and 0.18 V, corresponding to the progressive lithiation of the branched nanowires and the formation of a series of Li-Ge alloys (a-$Li_xGe \rightarrow$ a-$Li_{15}Ge_4 \rightarrow$ c-$Li_{15}Ge_4$).[57,58] The consistency in the potential and intensity of these

reduction peaks is illustrated in the contour plot showing the DCPs from the 2nd to the 25th charge in Figure 5(d). A sharp oxidation peak at ~ 0.51 V was observed in the DCP for the first discharge, as shown in Figure 5(c), corresponding to the delithiation of the c-$Li_{15}Ge_4$ phase.[59] The potential of this peak does not significantly vary with increased cycling as can be seen in the contour plot showing the DCPs from the 2nd to the 25th discharge (Figure 5(e)).

The specific capacity values achieved from the GeSn branched nanostructures are greater than[60–66] or comparable to[67–70] previously reported values for other Ge nanowire based anode materials. As there has been no report on the capacities of GeSn nanowires we are unable to make a comparision to GeSn nanowires, however these GeSn branched nanostructures show slight improvement over GeSn nanocrystals with similar Sn incorporation (x = 0.05).[34] We propose that the remarkable specific capacities and the high ICE obtained with the GeSn branched nanostructures are due to the nanoscale branches which are protruding from large nanowire trunks. The nanoscale diameter (~40 nm) of the branches may allow for relatively short Li^+ ion diffusion path lengths, compared to unbranched nanowires, which in turn may result in a high ICE and increased voltage stability, as shown in the DCPs. Additionally, GeSn based nanostructures offers cost-reduction in terms of anode materials production compared to pure Ge based material. The impressive electrochemical performance of the GeSn branched nanostructure in terms of voltage stability, capacity retention and high specific capacity values demonstrates that they are a very promising anode material for Li-ion batteries.

Conclusion

The fabrication of novel GeSn branched nanowires has been achieved through a single step VLS growth mechanism. This branching phenomenon of GeSn nanowires maintains epitaxy

with the primary "trunk" crystal and retains its structural quality without any apparent crystal defects. A proposed growth mechanism has been described for the fabrication of these GeSn nanostructures, outlining the role of sidewall wetting by Sn in the self-catalysation of the nanowire branches. A particular set of catalyst, precursor and precursor concertation was required for sidewall wetting by Sn, as a result of deposition and precipitation from the vapour phase and liquid catalytic seeds at the tip of the nanowire trunks. The simple nature of the growth has the potential to lend itself to heightened control of branched nanowire structures if more restrictions and parameters could be in place during growth, *e.g.* flux control. In-situ experiments may be required to conclude the specific source of sidewall Sn, which in turn could lead to precise engineering over the highly ordered 3D nanostructures. The branched GeSn nanowires, while chemically a homostructure, have the potential to act as semiconducting heterojunction due the possibility of having different bandgaps resulting from the variation of Sn content in the different segments of the nanostructures. Furthermore, the GeSn branched nanowires exhibit suitability as an anode material in Li ion batteries, due to the short Li^+ ion diffusion path lengths in the nanowire branches. Specific capacity for the branched nanowires were found to be either comparable to, or surpass, previously reported values for other Ge based anodes, demonstrating the capability of these materials for use in Li-ion batteries. We believe that further enhancement in Sn incorporation and a reduction in trunk dimension will improve the application of GeSn branched nanostructures in Li-ion batteries.

Acknowledgement

This research was funded by Science Foundation Ireland (Grant No: 14/IA/2513), and by the Irish Research Council through a Postgraduate Scholarship to JD (Grant No.:

GOIPG/2015/2772). We would like to acknowledge the Advanced Microscopy Laboratory, Trinity College Dublin, for their contribution to the imaging, and Prof. Andrea Falqui, King Abdullah University of Science and Technology for his contribution to the EDX analysis.

References

1 Z. Li, H. Yang, F. Wu, J. Fu, L. Wang and W. Yang, *Electron. Mater. Lett.*, 2017, **13**, 174–178.

2 H. Wu, Y. Yang, E. Oh, F. Lai and D. Yu, *Nanotechnology*, 2012, **23**, 265602.

3 M. J. Bierman, Y. K. A. Lau and S. Jin, *Nano Lett.*, 2007, **7**, 2907–2912.

4 G. K. Mor, O. K. Varghese, M. Paulose, K. Shankar and C. A. Grimes, *Sol. Energy Mater. Sol. Cells*, 2006, **90**, 2011–2075.

5 Changdong Gu, Chun Cheng, Haiyou Huang, Tailun Wong, Ning Wang, and Tong-Yi Zhang, *Cryst. Growth Des.*, 2009, **9**, 3278–3285.

6 G. Flynn, K. Palaniappan, M. Sheehan, T. Kennedy and K. M. Ryan, *Nanotechnology*, **28,** (2017).

7 C. Cheng and H. J. Fan, *Nano Today*, 2012, **7**, 327–343.

8 T. Kennedy, M. Bezuidenhout, K. Palaniappan, K. Stokes, M. Brandon and K. M. Ryan, *ACS Nano*, 2015, **9**, 7456–7465.

9 X. Jiang, B. Tian, J. Xiang, F. Qian, G. Zheng, H. Wang, L. Mai and C. M. Lieber, *Proc. Natl. Acad. Sci. U. S. A.*, 2011, **108**, 12212–12216.

10 K. A. Dick, K. Deppert, M. W. Larsson, T. Mårtensson, W. Seifert, L. R. Wallenberg and L. Samuelson, *Nat. Mater.*, 2004, **3**, 380–384.

11 J. Hou, X. Yang, X. Lv, D. Peng, M. Huang and Q. Wang, *Appl. Surf. Sci.*, 2011, **257**, 7684–7688.

12 A. L. Beaudry, J. M. Laforge, R. T. Tucker, J. B. Sorge, N. L. Adamski, P. Li, M. T. Taschuk and M. J. Brett, *Nano Lett.*, 2014, **14**, 1797–1803.

13 A. L. Beaudry, J. M. Laforge, R. T. Tucker, P. Li, M. T. Taschuk and M. J. Brett, *Cryst. Growth Des.*, 2013, **13**, 212–219.

14 M. Rauber, I. Alber, S. Muöller, R. Neumann, O. Picht, C. Roth, A. Schoökel, M. E. Toimil-Molares and W. Ensinger, *Nano Lett.*, 2011, **11**, 2304–2310.

15 S. H. Lee, Y. R. Jo, Y. Noh, B. J. Kim and W. B. Kim, *J. Power Sources*, 2017, **367**, 1–7.

16 P. Schönherr and T. Hesjedal, *Chem. - A Eur. J.*, 2016, **22**, 13823–13825.

17 R. Soref, *Nat. Photonics*, 2010, **4**, 495–497.

18 S. Zaima, O. Nakatsuka, T. Asano, T. Yamaha, S. Ike, A. Suzuki, K. Takahashi, Y. Nagae, M. Kurosawa, W. Takeuchi, Y. Shimura and M. Sakashita, *2016 IEEE Photonics Soc. Summer Top. Meet. Ser. SUM 2016*, 2016, **16**, 37–38.

19 J. Zheng, Z. Liu, C. Xue, C. Li, Y. Zuo, B. Cheng and Q. Wang, *J. Semicond.*, 2018, **39**, 1–6.

20 S. Gupta, X. Gong, R. Zhang, Y. C. Yeo, S. Takagi and K. C. Saraswat, *MRS Bull.*, 2014, **39**, 678–686.

21 J. D. Sau and M. L. Cohen, *Phys. Rev. B - Condens. Matter Mater. Phys.*, 2007, **75**, 1–7.

22 D. W. Jenkins and J. D. Dow, *Phys. Rev. B*, 1987, **36**, 7994–8000.

23 V. Richard D'Costa, W. Wang, Q. Zhou, E. Soon Tok and Y. C. Yeo, *Appl. Phys. Lett.*, **104,** (2014).

24 F. Pezzoli, A. Giorgioni, D. Patchett and M. Myronov, *ACS Photonics*, 2016, **3**, 2004–2009.

25 S. A. Ghetmiri, W. Du, J. Margetis, A. Mosleh, L. Cousar, B. R. Conley, L. Domulevicz, A. Nazzal, G. Sun, R. A. Soref, J. Tolle, B. Li, H. A. Naseem and S. Q. Yu, *Appl. Phys. Lett.*, 2014, **105**, 6–11.

26 H. Mahmodi, M. R. Hashim, M. Kim, W. Fan, J.-H. Seo, Z. Liu, J. Wen, X. Zhang, T. Maeda, W. Jevasuwan, H. Hattori, H. Z. Xi, B. Y. Man, C. S. Chen, R. Yoshimine, K. Toko, T. Suemasu, N. Chen, G. Lin, L. Zhang, C. Li, S. Chen, W. Huang, J. Xu and J. Wang, *Jpn. J. Appl. Phys*. **56,** (2017).

27 A. Mosleh, S. A. Ghetmiri, B. R. Conley, M. Hawkridge, M. Benamara, A. Nazzal, J. Tolle, S.-Q. Yu and H. A. Naseem, *J. Electron. Mater.*, 2014, **43**, 938–946.

28 M. R. Bauer, J. Tolle, C. Bungay, A. V. G. Chizmeshya, D. J. Smith, J. Menéndez and J. Kouvetakis, *Solid State Commun.*, 2003, **127**, 355–359.

29 R. Ragan, C. C. Ahn and H. a. Atwater, *Appl. Phys. Lett.*, 2003, **82**, 3439–3441.

30 S. Gupta, R. Chen, Y. C. Huang, Y. Kim, E. Sanchez, J. S. Harris and K. C. Saraswat, *Nano Lett.*, 2013, **13**, 3783–3790.

31 M. S. Seifner, F. Biegger, A. Lugstein, J. Bernardi and S. Barth, *Chem. Mater.*, 2015, **27**, 6125–6130.

32 M. S. Seifner, S. Hernandez, J. Bernardi, A. Romano-Rodriguez and S. Barth, *Chem. Mater.*, 2017, **29**, 9802–9813.

33 T. Haffner, M. Zeghouane, F. Bassani, P. Gentile, A. Gassenq, F. Chouchane, N. Pauc, E. Martinez, E. Robin, S. David, T. Baron and B. Salem, *Phys. Status Solidi*, 2017, **215**, 1700743.

34 Y. J. Cho, C. H. Kim, H. S. Im, Y. Myung, H. S. Kim, S. H. Back, Y. R. Lim, C. S. Jung, D. M. Jang, J. Park, S. H. Lim, E. H. Cha, K. Y. Bae, M. S. Song and W. Il Cho,

Phys. Chem. Chem. Phys., 2013, **15**, 11691–11695.

35 R. J. A. Esteves, M. Q. Ho and I. U. Arachchige, *Chem. Mater.*, 2015, **27**, 1559–1568.

36 K. Ramasamy, P. G. Kotula, A. F. Fidler, M. T. Brumbach, J. M. Pietryga and S. A. Ivanov, *Chem. Mater.*, 2015, **27**, 4640–4649.

37 A. A. Tonkikh, N. D. Zakharov, A. A. Suvorova, C. Eisenschmidt, J. Schilling and P. Werner, *Cryst. Growth Des.*, 2014, **14**, 1617–1622.

38 D. Wang, F. Qian, C. Yang, Z. Zhong and C. M. Lieber, *Nano Lett.*, 2004, **4**, 871–874.

39 X. Liu, Y. Lin, S. Zhou, S. Sheehan and D. Wang, *Energies*, 2010, **3**, 285–300.

40 E. Mullane, T. Kennedy, H. Geaney, C. Dickinson and K. M. Ryan, *Chem. Mater.*, 2013, **25**, 1816–1822.

41 P. B. Sorokin, A. G. Kvashnin, D. G. Kvashnin, J. A. Filicheva, P. V. Avramov, A. S. Fedorov and L. A. Chernozatonskii, *ACS Nano*, 2010, **4**, 2784–2790.

42 J. Doherty, S. Biswas, D. Saladukha, Q. Ramasse, T. S. Bhattacharya, A. Singha, T. J. Ochalski and J. D. Holmes, *J. Mater. Chem. C*, 2018, 8738–8750.

43 S. Biswas, J. Doherty, D. Saladukha, Q. Ramasse, D. Majumdar, M. Upmanyu, A. Singha, T. Ochalski, M. A. Morris and J. D. Holmes, *Nat. Commun.*, 2016, **7**, 11405.

44 R. R. Lieten, C. Fleischmann, S. Peters, N. M. Santos, L. M. Amorim, Y. Shimura, N. Uchida, T. Maeda, S. Nikitenko, T. Conard, J.-P. Locquet, K. Temst and a. Vantomme, *ECS J. Solid State Sci. Technol.*, 2014, **3**, P403–P408.

45 W. Dou, B. Alharthi, P. C. Grant, J. M. Grant, A. Mosleh, H. Tran, W. Du, M. Mortazavi, B. Li, H. Naseem and S.-Q. Yu, 2018, **8**, 3220–3229.

46 H. Jagannathan, M. Deal, Y. Nishi, J. Woodruff, C. Chidsey and P. C. Mclntyre, *J.*

Appl. Phys., **100,** (2006).

47 S. Biswas, J. Doherty, D. Majumdar, T. Ghoshal, K. Rahme, M. Conroy, A. Singha, M. a. Morris and J. D. Holmes, *Chem. Mater.*, 2015, **27**, 3408–3416.

48 S. Biswas, C. O'Regan, N. Petkov, M. a. Morris and J. D. Holmes, *Nano Lett.*, 2013, **13**, 4044–4052.

49 J. F. Li, P. A. Agyakwa and C. M. Johnson, *J. Electron. Mater.*, 2014, **43**, 983–995.

50 V. A. Baheti, S. Kashyap, P. Kumar, K. Chattopadhyay and A. Paul, *Philos. Mag.*, 2018, **98**, 20–36.

51 D. Lv, M. L. Gordin, R. Yi, T. Xu, J. Song, Y. B. Jiang, D. Choi and D. Wang, *Adv. Funct. Mater.*, 2014, **24**, 1059–1066.

52 X. H. Liu, S. Huang, S. T. Picraux, J. Li, T. Zhu and J. Y. Huang, *Nano Lett.*, 2011, **11**, 3991–3997.

53 R. A. Dileo, S. Frisco, M. J. Ganter, R. E. Rogers, R. P. Raffaelle and B. J. Landi, *J. Phys. Chem. C*, 2011, **115**, 22609–22614.

54 E. Mullane, T. Kennedy, H. Geaney and K. M. Ryan, *ACS Appl. Mater. Interfaces*, 2014, **6**, 18800–18807.

55 D. McNulty, H. Geaney, D. Buckley and C. O'Dwyer, *Nano Energy*, 2018, **43**, 11–21.

56 T. Kennedy, E. Mullane, H. Geaney, M. Osiak, C. O'Dwyer and K. M. Ryan, *Nano Lett.*, 2014, **14**, 716–723.

57 L. Baggetto and P. H. L. Notten, *J. Electrochem. Soc.*, 2009, **156**, A169.

58 L. Baggetto, E. J. M. Hensen and P. H. L. Notten, *Electrochim. Acta*, 2010, **55**, 7074–7079.

59 K. Stokes, H. Geaney, G. Flynn, M. Sheehan, T. Kennedy and K. M. Ryan, *ACS Nano*, 2017, **11**, 10088–10096.

60 T. Qiang, J. Fang, Y. Song, Q. Ma, M. Ye, Z. Fang and B. Geng, *RSC Adv.*, 2015, **5**, 17070–17075.

61 W. Guo, L. Mei, Q. Feng and J. Ma, *Mater. Chem. Phys.*, 2015, **168**, 6–9.

62 H. S. Choe, S. J. Kim, M. C. Kim, D. M. Kim, G. H. Lee, S. B. Han, D. H. Kwak and K. W. Park, *RSC Adv.*, 2016, **6**, 72926–72932.

63 W. Li, Z. Yang, J. Cheng, X. Zhong, L. Gu and Y. Yu, *Nanoscale*, 2014, **6**, 4532–4537.

64 A. M. Chockla, K. C. Klavetter, C. B. Mullins and B. A. Korgel, *ACS Appl. Mater. Interfaces*, 2012, **4**, 4658–4664.

65 X. Xiao, X. Li, S. Zheng, J. Shao, H. Xue and H. Pang, *Adv. Mater. Interfaces*, **4,** (2017).

66 L. C. Yang, Q. S. Gao, L. Li, Y. Tang and Y. P. Wu, *Electrochem. commun.*, 2010, **12**, 418–421.

67 T. Kennedy, M. Brandon and K. M. Ryan, *Adv. Mater.*, 2016, 5696–5704.

68 X. Li, Z. Yang, Y. Fu, L. Qiao, D. Li, H. Yue and D. He, *ACS Nano*, 2015, **9**, 1858–1867.

69 T. D. Bogart, A. M. Chockla and B. A. Korgel, *Curr. Opin. Chem. Eng.*, 2013, **2**, 286–293.

70 D. McNulty, A. Lonergan, S. O'Hanlon and C. O'Dwyer, *Solid State Ionics*, 2018, **314**, 195–203.

Figures:

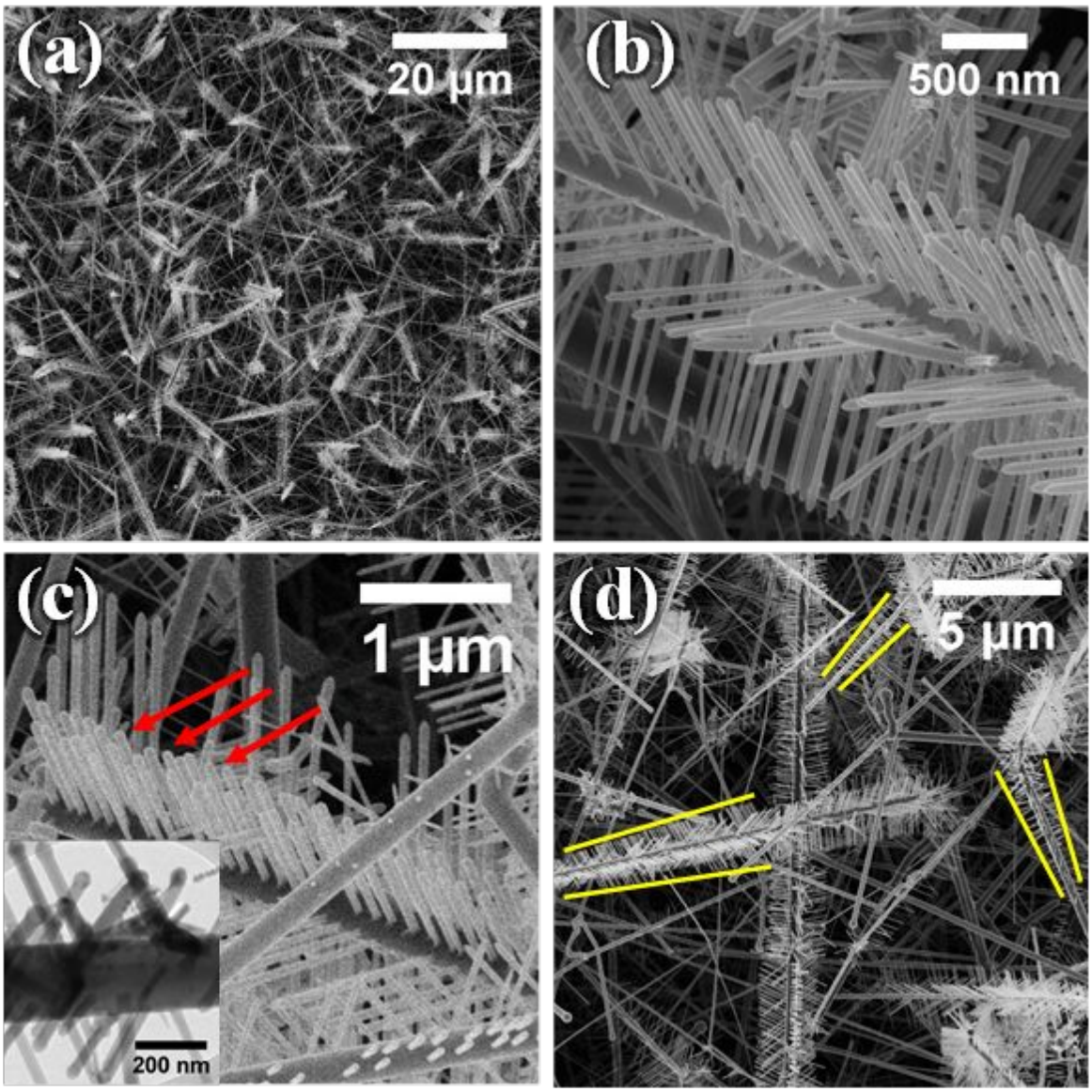

Figure 1: SEM images showing (a) the high yield of branched nanowires formed on an Si growth substrate. The branched nanowire shown in image (b) is typical of the those grown in this study, with highly oriented branches along the main trunk. The presence of spherical seeds on the branches, circled in red in (c), was not observed in all cases (*i.e.* no apparent seed in (b)). The yellow lines shown in image (d) indicate the increasing length of the branches along the length of the trunk (from tip to end).

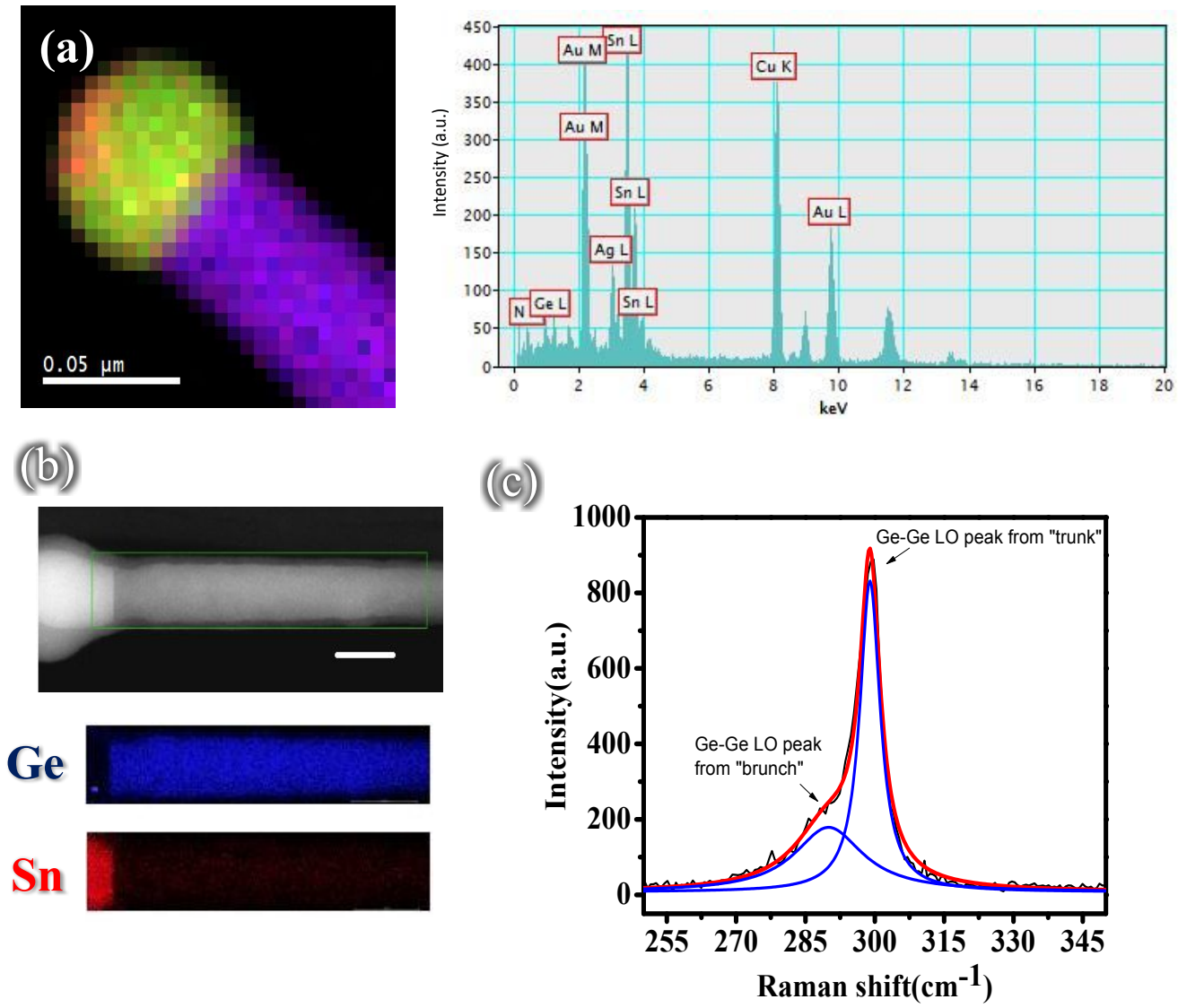

Figure 2: Elemental Analysis of the branched nanostructures. An elemental map (a) details the presence of Sn (green) and Au (red) in the tip of a nanowire trunk, with the trunk nanowire body mainly comprised of Ge (purple). Attached EDX spectrum from the seed part of the nanowire trunk displays the presence of Au and Ag metal in the nanowire tip. (b) Elemental maps of the branch segment of the nanostructure shows uniform Sn distribution in the nanowire with Sn catalyst at the tip (scale bar in HAADF STEM image corresponds to 20 nm). Room temperature Raman spectrum for a branched nanostructure recorded with an excitation

wavelength of 488 nm is shown in (c). Raman spectrum displays two distinct peaks, relating to the varying Sn content between nanowire trunk (4.4 at. % Sn) and branch (8.0 at. % Sn).

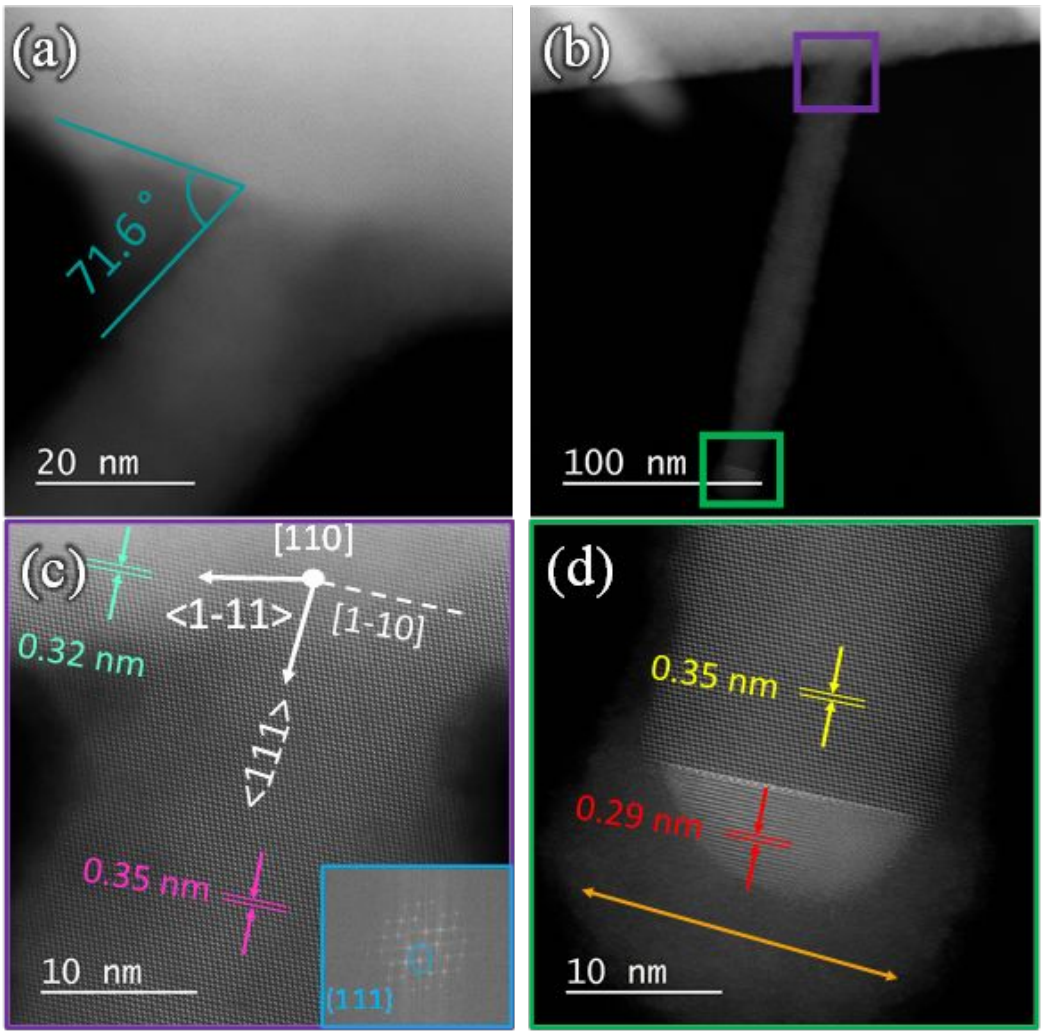

Figure 3: HRSTEM analysis of the branched nanowires. A branch protruding from a larger trunk can be seen in images (a) and (b). The angle between the <111> oriented trunk and branch as measured is 71.6 °. A high resolution image of the area near the branch-trunk interface (indicated by the purple box in (b)) can be seen in part (c), displaying the retention of

the crystal growth direction between the trunk and the branch. The nanowires are <111> oriented, as determined by FFT analysis (inset, blue box). The tip of this branch (green box) can be seen clearly in high resolution in image (d). There is a sharp interface between the small, hemispherical seed and the body of the nanowire.

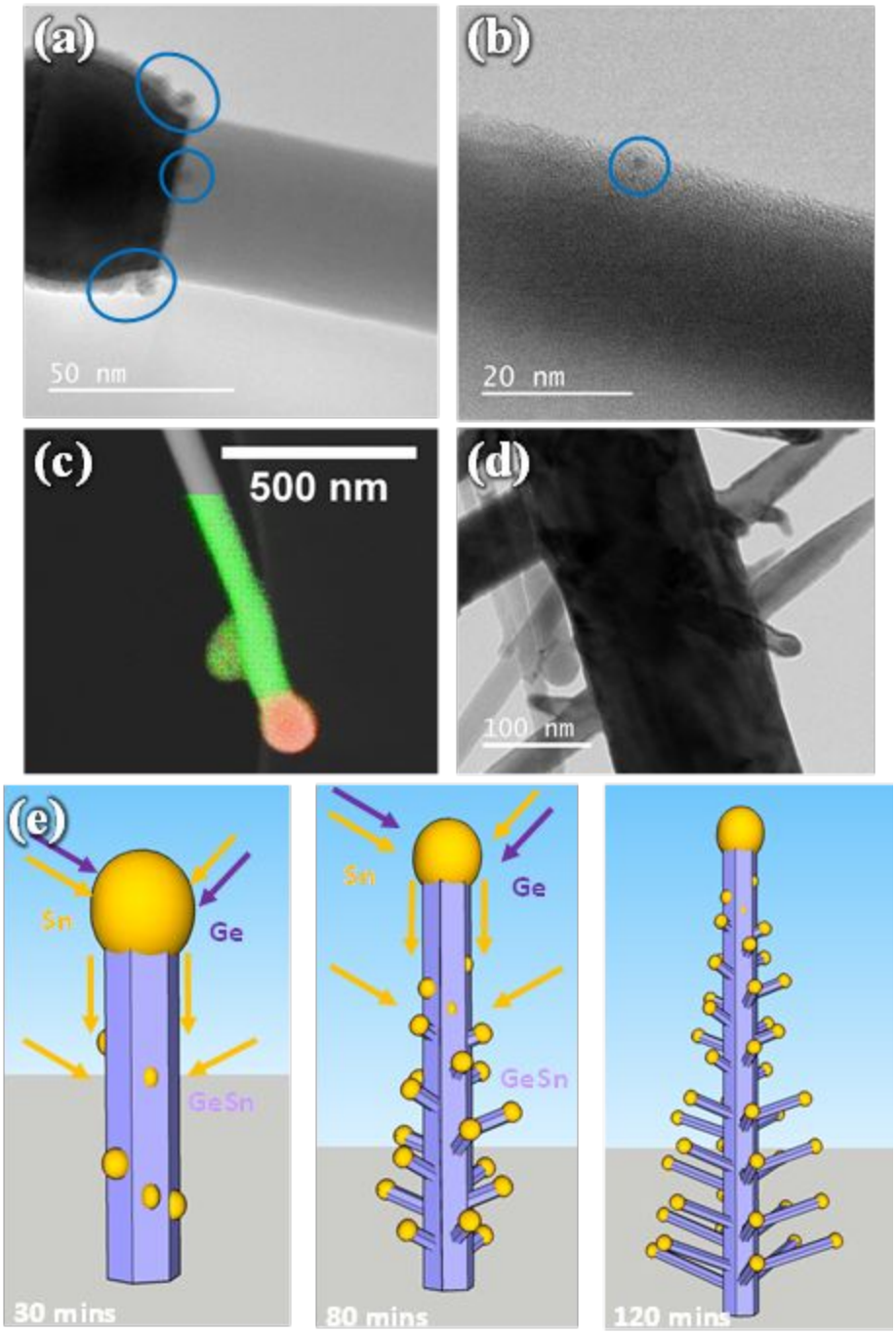

Figure 4: TEM and an EDX elemental map for the 30 min nanowire growth times are shown in images (a), (b) and (c) respectively. The TEM analysis reveals Sn particles and Sn segregation (marked with blue circles) on the surfaces of the trunk nanowires, as also confirmed by EDX mapping. (d) shows a representative TEM image for branched nanostructure after 80 min growth time. Schematics of the nanostructures at different growth times of 30, 80 and 120 mins are shown in (e).

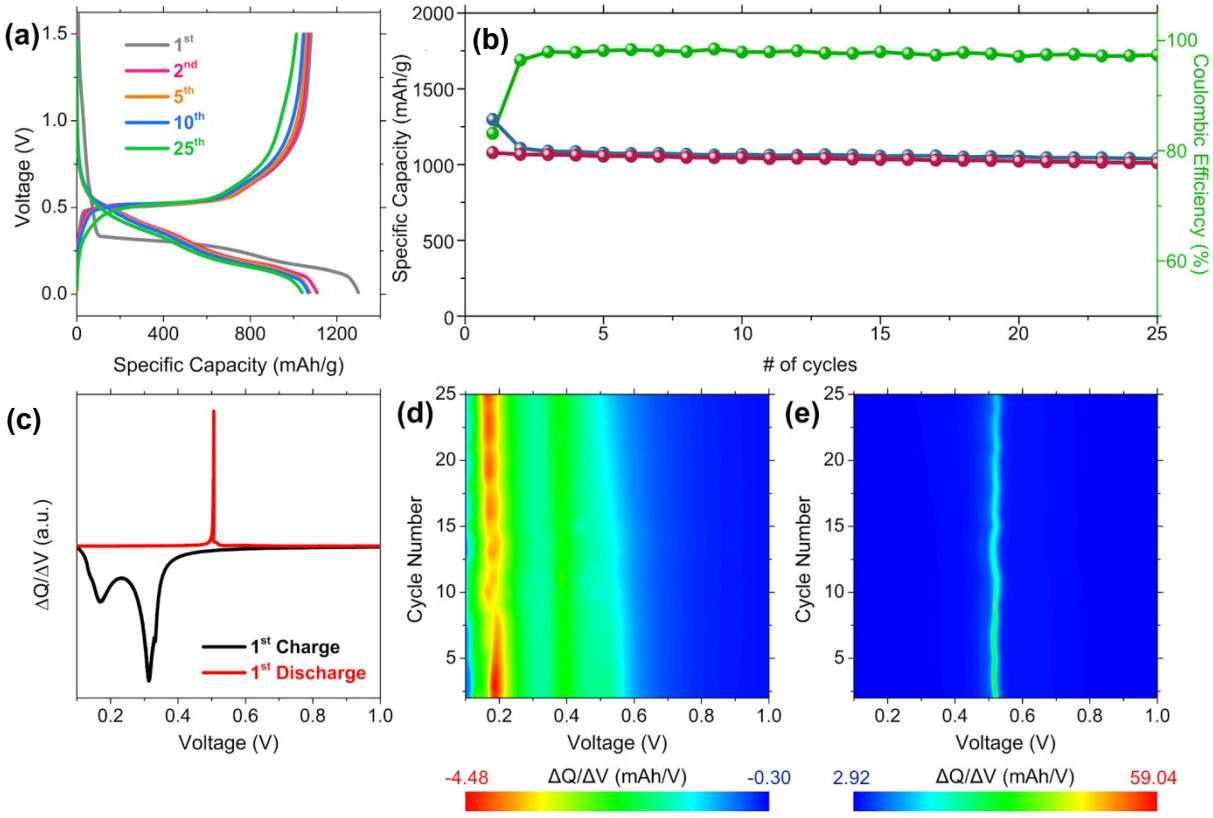

Figure 5: (a) Charge and discharge voltage profiles for the 1st, 2nd, 5th, 10th and 25th cycles for branched GeSn nanowires cycled at 0.2 C, in a potential window of 1.50 – 0.01 V (vs Li/Li+). (b) Charge and discharge capacity values and coulombic efficiencies obtained for branched GeSn nanowires IO over 25 cycles. (c) . Differential capacity plots (DCPs) for the 1st charge

and discharge. Differential capacity contour plots (part (d) and (e)) calculated from (a) charge curves and (b) discharge curves for a branched GeSn nanowires cycled at 0.2 C, from the 2nd to the 25th cycle.